Heuristic Modification of an Anatomical Markov Prior Improves its Performance

Kathleen Vunckx, Johan Nuyts
Dept. of Nuclear Medicine, K.U. Leuven, B-3000 Leuven, Belgium.

***Abstract*—Including anatomical information during emission tomography reconstruction with resolution modeling can enhance the image quality. Often accurate segmentation of the anatomical image is required, being a major challenge for most applications. Recently, we studied a segmentation-free MAP algorithm proposed by Bowsher et al, that encourages similar activity in a selection of neighboring voxels that look most alike in the anatomical image. In an evaluation with Monte Carlo simulations, it was found to be very promising for both bias and noise reduction in 3D PET/MRI brain imaging, compared to MLEM and MAP algorithms with regular or anatomical priors. Here we study a small modification of the Bowsher algorithm to further improve its reconstruction capacities. Comparison between the two methods using the same brain phantom scan simulations indicated a further decrease in bias at the same noise level.**

I. Introduction

Emission tomography projection images are subject to high statistical noise. Using maximum likelihood iterative reconstruction (MLEM), this Poisson noise can be modeled to avoid artifacts in the reconstruction image. However, the resulting images are often still very noisy. Many strategies have been proposed for noise reduction. The most popular ones are: (1) run MLEM until convergence and post-smooth with a low-pass filter; (2) maximum a posteriori (MAP) reconstruction using a prior function that encourages (locally) smooth images; (3) MAP reconstruction using an anatomical prior. In combination with a sufficiently accurate model for the finite spatial resolution of the PET (or SPECT) system, this latter approach achieves very strong (but position dependent) partial volume effect corrections. In this work, we will focus on one specific anatomical prior and compare it to the other two strategies.

In [1], Bowsher et al. proposed an anatomical prior that encourages smoothness in the emission image within local neighborhoods of voxels that are most similar in the anatomical image. This method has the advantage of not requiring segmentation. Therefore, subtle local differences, which are ignored by current segmentation methods, could possibly be exploited by this method. In this work, a comparison of two versions of the Bowsher prior is presented.

II. Theory

The reconstruction method proposed by Bowsher et al. [1] can be written as a typical MAP algorithm that applies a Markov prior to a group of neighbors. Hence, an objective function $\Phi(\Lambda, Q)$ is maximized, with Λ the emission image and Q the measured projection data:

$$\Phi(\Lambda, Q) = L(Q|\Lambda) - \beta M(\Lambda) \tag{1}$$

$L(Q|\Lambda)$ is the Poisson log-likelihood function, β is the regularization parameter, and $M(\Lambda)$ is the log-prior function:

$$M(\Lambda) = \sum_j \sum_k w_{jk} M_{jk} \tag{2}$$

where M_{jk} is the logarithm of the Markov prior to be applied to voxel j and its neighbor k, which is weighted by w_{jk}. The only difference to a regular Markov prior is the neighbors section. In contrast to using a shift-invariant neighborhood N, a voxel-dependent subset of neighbors N_j is selected from N based on the corresponding voxel values in the anatomical image. The idea is to encourage similar emission values in those voxels that are most alike in the anatomical image. For the selection of the neighbors, the weights w_{jk} are defined as

$$w_{jk} = 1, \quad \text{if} \quad k \in N_j \tag{3}$$

$$= 0, \quad \text{otherwise.} \tag{4}$$

Note that N_j and therefore also w_{jk} only depend upon the anatomical image. Hence, the neighbors selection of each voxel can be performed beforehand, stored (e.g. as the discriminating difference in the anatomical image) and reused in every iteration.

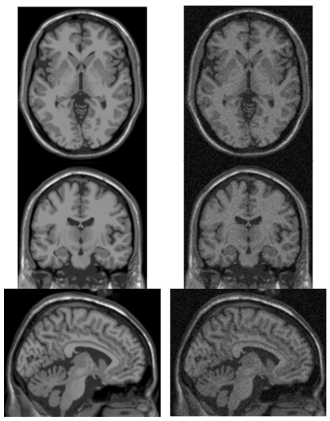

Fig. 1. Three orthogonal slices through the simulated noise-free (left) and noisy MRI image (right).

This work is supported by SBO grant 060819 "Quantiviam" of IWT, by IAP-grant P6/38 of the Belgian Science Policy, and by Research Foundation - Flanders.

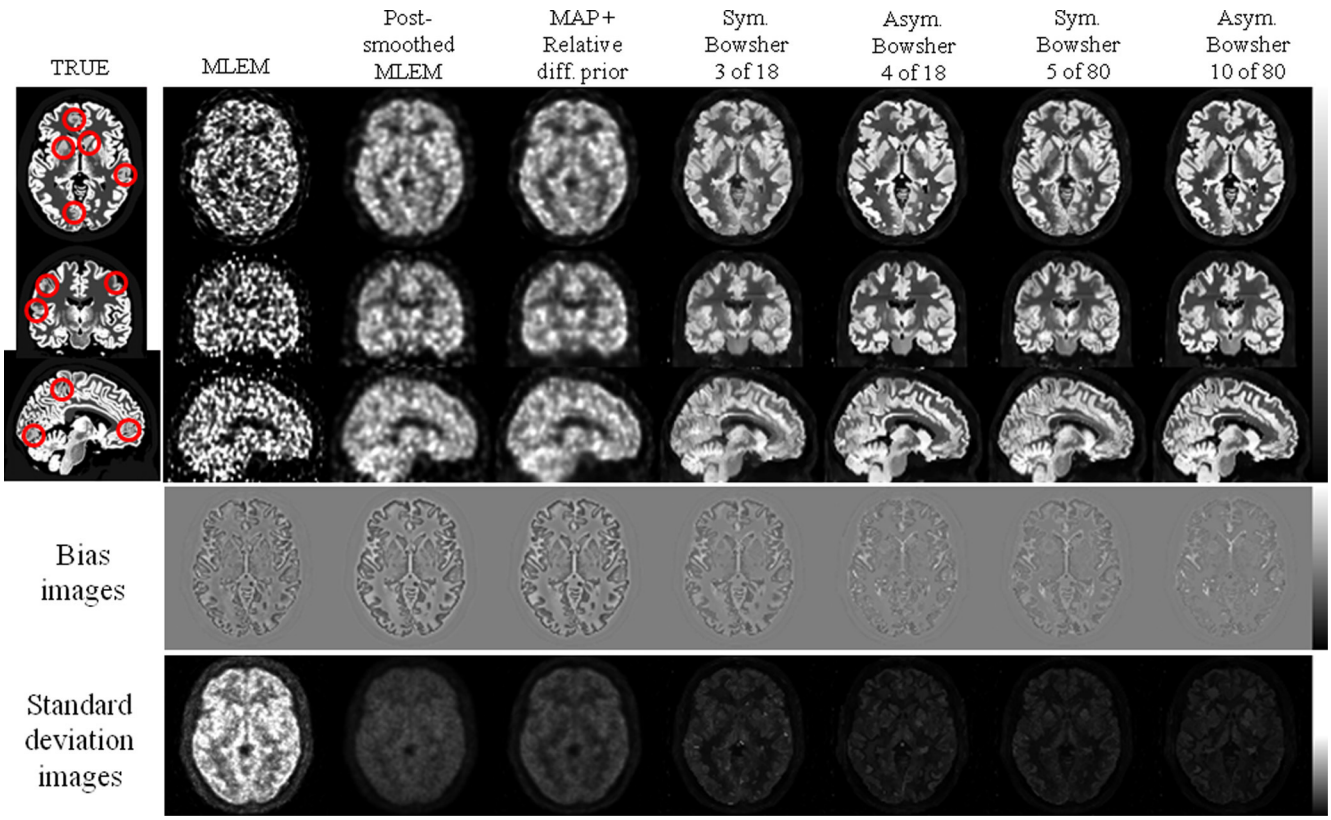

Fig. 2. Three orthogonal slices through the true activity distribution of the brain with hypointense lesions (top left), and through example reconstruction images obtained with the various algorithms (top right). The corresponding bias and standard deviation images are depicted on the two bottom rows. Each series of images was clipped at the same minimum and maximum value.

To maximize the objective function, the heuristic but effective gradient ascent algorithm proposed in [2] is used

$$\lambda_j = \lambda_j^{old} + \left(\frac{\partial L}{\partial \lambda_j} + \beta \frac{\partial M}{\partial \lambda_j}\right) / \left(\frac{\sum_i c_{ij}}{\lambda_j^{old}} - \beta \frac{\partial^2 M}{\partial \lambda_j^2}\right) \quad (5)$$

where all partial derivatives are evaluated in the current reconstruction λ_j^{old}. λ_j is the new activity estimate in voxel j and c_{ij} is the probability that a photon emitted from voxel j is detected in pixel i. The finite spatial resolution of the PET system must be taken into account when computing the values for c_{ij}.

The first derivative of the log-prior is

$$\frac{\partial M}{\partial \lambda_j} = \sum_k w_{jk} \frac{\partial M_{jk}}{\partial \lambda_j} + \sum_k w_{kj} \frac{\partial M_{kj}}{\partial \lambda_j} \quad (6)$$

Hence, even if voxel l is not a selected neighbor of j ($w_{jl} = 0$), it still can influence the gradient in voxel j when j is a selected neighbor of l ($w_{lj} = 1$). Therefore, we will refer to this prior as the *symmetrical* Bowsher prior. For appropriate choices of M, convergence to a global maximum is achievable, because the Hessian is semi-positive definite.

One could argue that since l is not a selected neighbor of j, it should not change the gradient (nor the activity) in voxel j. To achieve this, we defined an *asymmetrical* Bowsher prior by changing the gradient to

$$\frac{\partial M}{\partial \lambda_j} = \sum_k w_{jk} \frac{\partial M_{jk}}{\partial \lambda_j} \quad (7)$$

Unfortunately, no function M exists that satisfies (7), making proving convergence more complicated. However, our experience indicates convergence in practice.

III. Simulation Study

In a recent PET/MR brain imaging simulation study, we showed that the Bowsher prior strongly decreases the bias for a similar noise level when compared to post-smoothed MLEM [3]. In addition, it was shown to be competitive to a dedicated brain MAP reconstruction algorithm using perfect segmentation information, and superior to it when a realistic segmentation was used.

In the current study, we compared the symmetrical to the asymmetrical Bowsher prior, using the same realistic brain phantom and simulations, and the same figures of merit for reconstruction parameter optimization. Ten tissue images and the deduced noiseless and noisy T1-weighted MRI simulation were obtained from the Brainweb database [4], [5] (see Fig. 1). From these tissue images, a realistic PET activity distribution was built: one for a normal adult and one for a patient with 20 variably sized hypometabolic (25% decrease in uptake) gray matter (GM) lesions. Three orthogonal slices through the true PET activity distribution in the brain with hypointense lesions are shown in Fig. 2 (top left). The lesions visible in these slices were indicated by a red circle. All lesions were invisible in the MRI image. 60 PET projection data sets were simulated

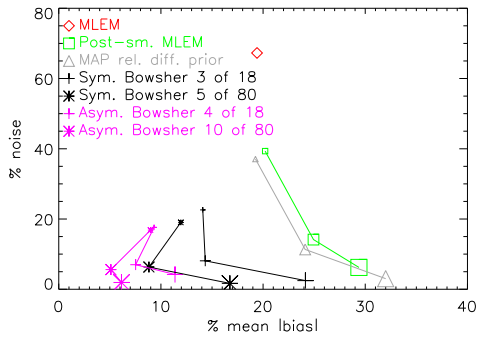

(a) Bias-noise analysis in the GM voxels in the normal brain

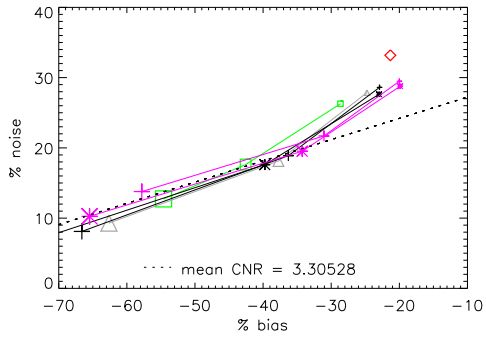

(b) Bias-noise analysis on the contrast in the lesion VOIs

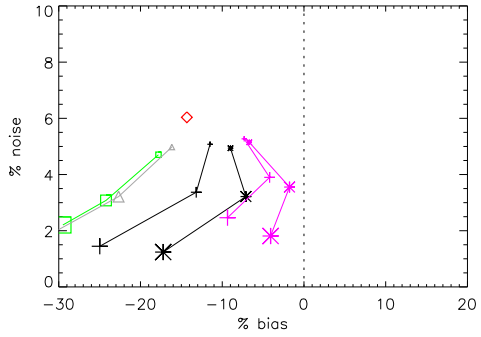

(c) Bias-noise analysis in the lesion VOIs in the normal brain

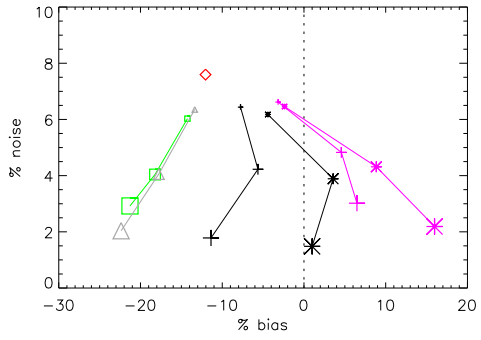

(d) Bias-noise analysis in the lesion VOIs in the diseased brain

Fig. 3. Bias-noise analysis of (a) the activity in the GM voxels of the normal brain, (b) of the contrast in the lesion VOIs, (c) of the activity in the lesion VOIs in the normal brain, and (d) in the brain with lesions. The Bowsher prior uses noise-free MRI image.

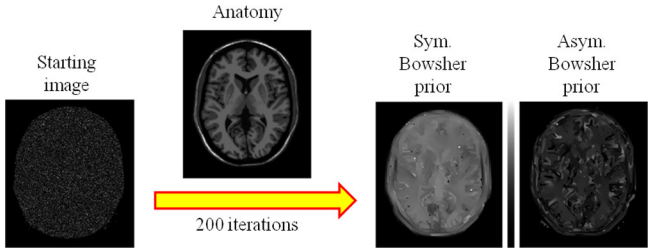

Fig. 4. Evaluation of the effect of applying the Bowsher prior only to a 2D starting image consisting of Poisson noise. 2 neighbors were selected from the 8 closest neighbors.

using the Monte Carlo SORTEO software [6], corresponding to 1-min FDG-PET scans.

Reconstruction parameters, such as β and the number of neighbors, were optimized using a figure of merit combining the normalized root mean squared error (NRMSE) on the activity in the GM voxels and on the mean contrast in the lesions (see [3] for more details). The contrast in a lesion was defined as the difference in mean activity in the lesion VOI in the normal brain and that in the diseased brain. The system resolution was modeled by a 3D Gaussian with a FWHM of 4.0 mm in the transaxial planes and 5.45 mm in the axial direction. Attenuation and scatter were also modeled during reconstruction, while randoms were ignored. Ordered subsets were used to accelerate convergence: 6×36, 2×16, 2×1 (global iterations × number of subsets, including the calculation of the starting image). The MAP and Bowsher reconstructions were started from a fast MLEM reconstruction (1 iteration over 36 subsets). All MAP reconstructions use the relative difference prior, as described in [2], with no increased tolerance for large edges (i.e. $\gamma = 0$). A bias-noise analysis was performed on these reconstructions.

To get more insight in the different behaviour of the two Bowsher priors, both types were applied on a 2D starting image consisting of Poisson noise (see Fig. 4):

$$\lambda_j = \lambda_j^{old} - \frac{\partial M}{\partial \lambda_j} / \frac{\partial^2 M}{\partial \lambda_j^2} \tag{8}$$

The anatomical image used as a priori information was a transaxial slice through the noise-free MRI image of the simulated brain. 200 iterations were performed.

Finally, the effect of noise in the anatomical image on the performance of both Bowhser priors was evaluated by repeating the Bowsher reconstructions of the 60 noisy PET sinograms using the MRI image with 9% noise of Fig. 1(right) as anatomical information, as well as the bias-noise analysis.

IV. Results

In order to perform a first, qualitative evaluation of the two Bowsher reconstruction methods, example reconstruction images of the same simulated 1-min scan are shown in Fig. 2 (top right). From left to right the following reconstruction algorithms were used (with optimized parameters): MLEM, post-smoothed MLEM, MAP with relative difference prior (RD-MAP), MAP with symmetrical Bowsher prior using 3 selected

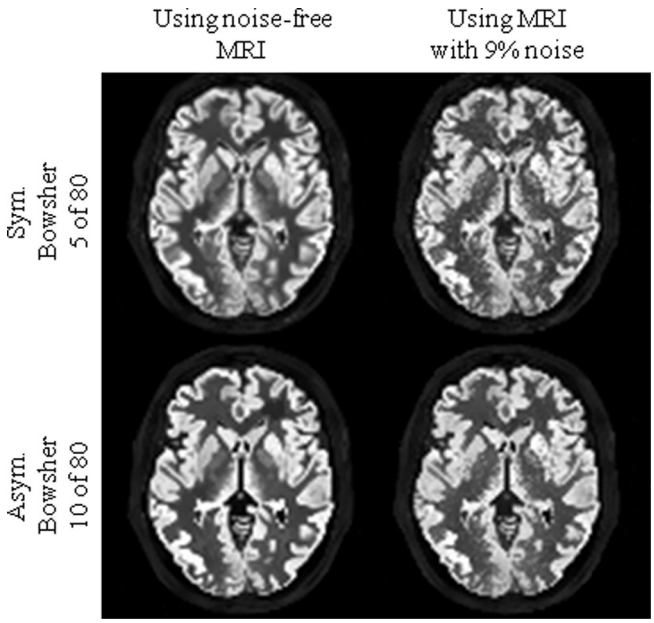

Fig. 5. Evaluation of the effect of using a noisy MRI image instead of a noise-free MRI image as a priori information during Bowsher reconstruction.

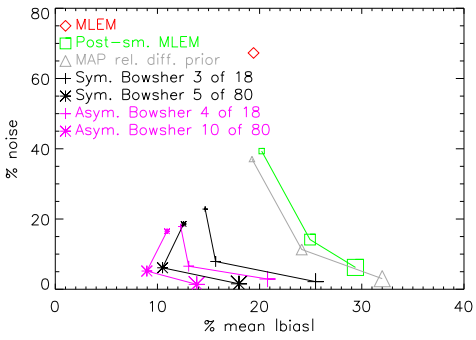

(a) Bias-noise analysis in the GM voxels in the normal brain

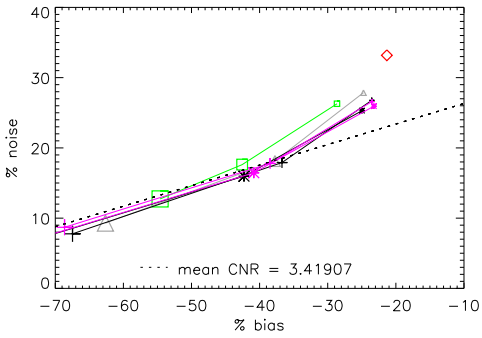

(b) Bias-noise analysis on the contrast in the lesion VOIs

Fig. 6. Bias-noise analysis (a) of the activity in the GM voxels of the normal brain and (b) of the contrast in the lesion VOIs. The Bowsher prior uses MRI image with 9% noise.

neighbors from 18 neighbors (3 of 18), MAP with asymmetrical Bowsher (4 of 18), and MAP with sym. and asym. Bowsher prior using a larger neighborhood (5/10 of 80). The Bowsher images look much sharper than the (post-smoothed) MLEM and RD-MAP images because of the intrinsic edge-preserving character of the priors. Although more neighbors were selected in the asymmetrical Bowsher prior, compared to the symmetrical one, typically sharper, but especially more homogeneous images were obtained. From the bias images in the next to last row of Fig. 2 a clear reduction in bias can be perceived in the symmetrical Bowsher reconstructions with respect to the MLEM and RD-MAP images. The bias was further reduced by the use of the asymmetrical prior rather than the symmetrical one, especially at the tissue transitions. Both versions induced a similar global decrease in standard deviation compared to the conventional algorithms (see last row of Fig. 2). The asymmetrical Bowsher images had lower noise at the edges of the GM at the cost of increased noise in the center of the white matter.

In Fig. 3(a), the percentage noise in the GM voxels is plotted versus the percentage mean absolute bias in these voxels. The red, green, gray, black and pink symbols show the results from unprocessed MLEM, post-smoothed MLEM (Gaussian with 3/6/9 mm FWHM), RD-MAP, symmetrical and asymmetrical Bowsher reconstruction, respectively. For the MAP reconstructions, the smallest and largest symbol denote the result for a 10-fold lower/higher β, compared to the optimized one. Both Bowsher algorithms yielded a clearly lower bias and noise in the GM than MLEM and RD-MAP. The asymmetrical one could further reduce the bias, while reaching the same noise level. Choosing a larger neighborhood, i.e. 80 (depicted by stars) instead of 18 neighbors (plus signs), had a similar impact.

In Fig. 3(b), the % bias and % noise on the contrast in the lesions, both averaged over all lesions, are presented in a graph. A similar mean contrast-to-noise level could be obtained with all reconstruction algorithms, except for MLEM without post-processing.

Fig. 3(c) and (d) plot the mean % noise on the lesion activity as a function of the mean % bias on this activity in the normal brain and the brain with lesions, respectively. As in the rest of the GM voxels, bias was reduced by using the Bowsher algorithms. The noise level was comparable to that of post-smoothed MLEM and RD-MAP. Both using a larger neighborhood and using the asymmetrical version of the Bowsher prior resulted in a reduction of the negative bias. In the brain with lesions, the bias became even slightly positive.

To facilitate the interpretation of the differences in outcome when using the symmetrical or the asymmetrical Bowsher prior, the prior-only-based 'reconstructions', shown in Fig. 4 (right images), are analyzed. Although both images clearly show the influence of the exploited anatomical information, a much stronger smoothing only within the various tissues is apparent when applying the symmetrical Bowsher prior. This explains the sharper images as well as the reduced bias.

The above simulation study illustrates how much one can ideally gain in image quality with the Bowsher priors. However, typically the available MRI images will be noisy. Therefore, we repeated the analysis with a very noisy MRI image (see Fig. 1 (right)) as prior knowledge about the anatomy. In

Fig. 5 the reconstruction images yielded with the symmetrical (top row) and asymmetrical (bottom row) Bowsher algorithms using a large neighborhood are shown. For the reconstructions resulting in the left images the noise-free MRI image was used, whereas for the right images the information of the noisy MRI image was exploited. One can see that the noise of the MRI image appears to some extent in the PET reconstructions. It is most apparent in the white matter voxels in the symmetrical Bowsher reconstruction.

To quantitatively evaluate the effect of noise in the anatomical image, the new bias-noise analysis from Fig. 6 (based on the noisy MRI image) needs to be compared to the initial one shown in Fig. 3. One can observe a small increase in bias in the GM voxels for the symmetrical Bowsher method, and a more pronounced increase in bias in these voxels for the asymmetrical one. Nevertheless, the asymmetrical Bowsher still outperforms the symmetrical one. The difference in CNR in the lesion VOIs is negligible.

V. Discussion

Differences between the symmetrical and asymmetrical Bowsher reconstruction images will mainly appear near transitions from one anatomical structure to another. Indeed, in the former case, a voxel at the edge of an anatomical region can have many neighbors that are similar in the anatomical image, while also having some (non-selected) neighbors that are quite different, but that consider this voxel as one of its selected neighbors by lack of more similar ones. Therefore, compared to the asymmetrical Bowsher, the symmetrical one will suffer somewhat more from undesired regularization. The optimized number of neighbors was found to be systematically larger for the asymmetrical Bowsher. We believe this might be to compensate for the extra (unwanted) regularization in the symmetrical one.

The parameter optimization was not repeated for the Bowsher reconstructions that use the noisy MRI image as prior information instead of the noise-free MRI image. Such optimization might for instance propose a higher weight for the prior in order to suppress the noise in the reconstructed image. Possibly slightly improved bias-noise characteristics could have been obtained. However, this was considered out of the scope of this work, which was focused on highlighting the differences between the two types of Bowsher priors.

VI. Conclusion

Both Bowsher priors improve the visual and quantitative image quality compared to (post-smoothed) MLEM and MAP. The intuitively developed asymmetrical Bowsher prior outperforms the symmetrical one after individual parameter optimization. The differences are most apparent at anatomical edges (i.e., sharper edges for the asymmetrical Bowsher). The bias in the gray matter is reduced while preserving low noise. Its advantage becomes smaller if the MRI image suffers from a high noise level. The optimized number of selected neighbors is systematically larger for the asymmetrical Bowsher prior. Like the original Bowsher reconstruction algorithm, the asymmetrical one benefits from using larger neighborhoods, resulting in reduced bias at the same noise level.

References

[1] JE Bowsher, H Yuan, LW Hedlund, TG Turkington, G Akabani, A Badea, WC Kurylo, CT Wheeler, GP Cofer, MW Dewhirst, GA Johnson. "Using MRI information to estimate F18-FDG distributions in rat flank tumors", *IEEE Nucl Sci Symp Conf Record*, 2004, pp 2488-2492.

[2] J Nuyts, D Bequé, P Dupont, L Mortelmans. "A concave prior penalizing relative differences for maximum-a-posteriori reconstruction in emission tomography", *IEEE Trans Nucl Sci*, vol 49, no 1, pp 56-60, 2002.

[3] A Atre, K Vunckx, K Baete, A Reilhac, J Nuyts. "Evaluation of different MRI-based anatomical priors for PET brain imaging", *IEEE Nucl Sci Symp Conf Record*, 2009, pp 2774-2780.

[4] website: "http://www.bic.mni.mcgill.ca/brainweb/"

[5] DL Collins, AP Zijdenbos, V Kollokian, JG Sled, NJ Kabani, CJ Holmes, AC Evans. "Design and construction of a realistic digital brain phantom", *IEEE Trans Med Imaging*, vol 17, no 3, pp 463-468, 1998.

[6] A Reilhac, C Lartizien, N Costes, S Sans, C Comtat, RN Gunn, AC Evans. "PET-SORTEO: A Monte Carlo-based simulator with high count rate capabilities", *IEEE Trans Nucl Sci*, vol 51, no 1, pp 46-52, 2004.